## PAPER

# Fabricating multifunctional nanoparticle membranes by a fast layer-by-layer Langmuir–Blodgett process: application in lithium–sulfur batteries†

M. S. Kim,‡[ac] L. Ma,‡[b] S. Choudhury,[a] S. S. Moganty,[d] S. Wei[a] and L. A. Archer*[a]

The Langmuir–Blodgett technique is a powerful and widely used method for preparing coatings of amphiphilic molecules at air/water interfaces with thickness control down to a single molecule. Here, we report two new LB techniques designed to create ordered, multifunctional nanoparticle films. The methods utilize Marangoni stresses produced by surfactants at a fluid/solid/gas interface and self-assembly of nanoparticles to facilitate rapid creation of ultrathin films of carbon, metal-oxide nanoparticles, polymers, and combinations of these materials on any non-reactive support in a layer-by-layer configuration. Using polyolefin separators in lithium sulfur electrochemical cells as an example, we illustrate how the method can be used to create structured membranes for regulating mass and charge transport. We further show that a layered MWCNT/SiO$_2$/MWCNT nanomaterial created in a clip-like configuration, with gravimetric areal coverage of ~130 μg cm$^{-2}$ and a thickness of ~3 μm, efficiently intercept and reutilize dissolved lithium polysulfides for improving electrochemical performances of lithium sulfur batteries.

## 1. Introduction

The Langmuir–Blodgett (LB) technique is a method for preparing coatings of amphiphilic molecules at air/water interfaces with thickness of one molecule.[1–3] The method is attractive for a variety of reasons, including its ability to precisely control the thicknesses of coatings down to molecular dimensions, for the versatility of substrates that can be coated, and for its scalability. The LB technique has been applied in numerous fields of science and technology to form thin micro patterns,[4,5] monolayer films,[6,7] and monoparticle layers based on spheres,[8,9] rods,[10,11] and nanotubes,[12] which can be easily transferred onto various substrates. Nie *et al.* proposed an electrospray method that extends the LB technique to yield high coverage of metallic nanospheres at the surface of water.[13] With LB assembly it is therefore now possible to produce monolayers of colloidal films that broadly range in particle sizes and shapes, which may be used to advantage for tuning film properties[14] as well as to create thin film devices.[15,16]

This article reports two new and versatile LB coating approaches – Langmuir–Blodgett sequential dip coating (LBSDC) and the Langmuir–Blodgett scooping (LBS), which facilitate efficient creation of multifunctional, layer-by-layer coatings of carbon, metal-oxides, polymers, and combinations of these materials on any non-reactive substrate. Unlike the conventional LB method, which uses mechanical force applied to a disordered material at the air/water interface to create well-ordered assemblies of molecules or particles, LBSDC and LBS utilize surfactant and self-assembly, respectively, to create ordered coatings that can be transferred to a solid or porous support. This difference allows highly organized coatings to be formed in a fraction of the time and using any containment vessel (*i.e.* a LB trough is not required). The speed with which ordered monolayer coatings are created, the high quality and low thickness of the transferred coatings, and versatility of the process by which the coatings are formed mean that LBSDC and LBS can be applied in a repetitive fashion to fabricate multi-functional coatings in a layer-by-layer format that enable design of new materials with surface features able to regulate mass and charge transport. Because the assembly occurs at a sharp gas/liquid interface, the methods nonetheless benefit from the inherent attributes of the LB technique – precise control over

[a]*Department of Chemical and Biomolecular Engineering, Cornell University, Ithaca, New York 14853-5201, USA. E-mail: laa25@cornell.edu; Tel: +1 607 254 8825*

[b]*Department of Materials Science & Engineering, Cornell University, Ithaca, New York 14853-5201, USA*

[c]*Center for Energy Convergence, Korea Institute of Science and Technology, Hwarangno 14-gil 5, Seongbuk-gu, Seoul, 02792, Republic of Korea*

[d]*NOHMs Technologies, 1200 Ridgeway Ave. Suite 110, Rochester, NY, 14615, USA*

† Electronic supplementary information (ESI) available: Surface pressure profile measurements, versatility of the coating methods, electrochemical performance of modified separators, voltage profiles, impedance measurement, and cell configuration summary table are mentioned. See DOI: 10.1039/c6ta06018h

‡ These authors contributed equally to this work.

This journal is © The Royal Society of Chemistry 2016

*J. Mater. Chem. A*, 2016, **4**, 14709–14719 | 14709

film thickness and structure, as well as the versatility of substrate choices. Moreover, numbers and positions of suspension injection nozzle and water surface area can be altered and customized to scale up the coating process.

The utility of the LBSDC and LBS approaches is illustrated in the present study using the polyolefin separator membrane employed in standard lithium–sulfur (LiS) electrochemical cells. This choice is motivated by the promise such cells offer for cost-effective storage of large quantities of electrical energy and by the stubborn challenges associated with solubility and diffusion of long-chain ($Li_2S_x$; $x \geq 4$), lithium polysulfide (LiPS) species, to the electrolyte that limit performance of LiS batteries.[18-50] We report that using LBSDC and LBS it is possible to create multifunctional coatings in multiple designs that enable conventional membranes to overcome the most difficult challenges. We further report a novel "*clip*" separator membrane configuration in which a well-formed, but incomplete layer of structures of one chemistry is sandwiched between complete layers of another chemistry. This coating morphology allows one to engineer the surface of a membrane to simultaneously trap an undesired material (*e.g.* LiPS) and to maintain electrochemical access to it. In so doing, we show that it is possible to preserve the favorable attributes of the Li–S cell while addressing its most serious weaknesses.

## 2.  Experimental section

### 2.1  Synthesis

Silica nanospheres are synthesized by the Stober synthesis technique.[17] In this method, 10 ml of ammonium hydroxide, 10 ml of water and 75 ml of ethanol are taken in a round bottom flask and stirred using a stir bar to ensure proper mixing. Under smooth stirring conditions, 5.6 ml of tetraethyl orthosilicate (TEOS) is added drop-wise. After 12 hours of stirring, the prepared monodispersed silica nanospheres are purified by alternate centrifuging and sonication in an ethanol–water mixture until the colloidal solution reaches a stable pH of 7. The size of the prepared silica is characterized using scanning electron microscopy (SEM). The resulting silica nanospheres are determined by means of dynamic light scattering (DLS) and SEM analysis to be approximately 350 nm in diameter.

A LB film forming suspension is comprised of 3 wt% of a desired nanomaterial in pure ethanol (Decon, 200 Proof). To create the materials used in this study 3 wt% of silica nanosphere, titania nanopowder (rutile, 99% purity, Advanced Materials™), multi-walled carbon nanotube (L 6–9 nm × 5 μm, >95% carbon, Sigma Aldrich), Ketjen-Black carbon (Akzo Nobel), and Super-P carbon (TIMCAL) is dispersed in pure ethanol. Then each of the suspension is sonicated for 30 minutes to enhance the dispersion of the particles. Note that the ultimate coating quality is not sensitive to the weight composition of the nanomaterials in ethanol; 0.5 to 3 wt% of the nanomaterial suspensions yielded the same quality coatings. However, the film quality heavily depends on the distribution of the dispersed particle sizes; presence of aggregates or clusters will form defects during the self-assembly of LB films.

The sodium dodecyl sulfate (SDS) surfactant is made by dissolving 3 wt% of SDS in DI water.

### 2.2  Coating process

The commercial polypropylene separator (Celgard 2500) was cut into a 1.6 cm diameter circular disc. The disc is placed onto a 1.8 × 1.8 cm microscope cover glass, and the ends of the separator are taped with Kapton tape for the coating process.

Mono/multi layers of silica nanospheres, multi-walled carbon nanotubes (MWCNT), Ketjen Black (KB) carbon, and Super P (SP) carbon are coated on the separator using the LBS method. Prepared separators are washed with water to flush out any impurity specie stuck onto the surface. One drop of iso-propanol (IPA) is applied onto the separator or coated separator to enhance wetting by water, and the excess IPA diluted with water. Then, the fully wetted separator is immersed in water for the coating process. A chosen suspension is then injected at the surface of the water until more than half of the water surface is saturated with the desired nanomaterial; the separator is subsequently raised up to transfer the film followed by a constant injection of the suspension. After that, the coated separator is dried on a hot plate at 110 °C for 30 seconds. Note that IPA wetting step is not required for the silica nanospheres or hydrophilic surface coatings. The single layer coating process is repeated until the desired number of layers is achieved. After the final layer coating, the separator is dried on the hot plate at 110 °C for 1 minute. Video demonstration of LBSDC and LBS coatings are illustrated in ESI Videos.†

The clip coating is comprised of five coating layers of MWCNT, one layer of SP, three monolayers of silica nanospheres, and one final coating layer of MWCNT. The first five layers of MWCNT are coated in the same manner as the single component separator coating. Then, one layer of SP, which acts as an adhesion layer for the silica nanospheres, is coated on top of MWCNT using the LBS method. ∼90% of the MWCNT and SP carbon coated separator is covered with three monolayers of silica nanospheres using the LBSDC method. During the silica coating, IPA is only applied for the first coating layer. For the final layer of MWCNT, the remaining ∼10% of the separator is wetted with IPA. And after the dilution of IPA, the whole surface of the separator is coated with one layer of MWCNT using LBS. The clip coated separator is then dried on the hot plate at 110 °C for 1 minute.

### 2.3  Battery preparation

**LiS cathodes.** ISC (Infused Sulfur Cathode) – sulfur infused in KB carbon composite was prepared by an infusion method. First, sulfur powder (Sigma Aldrich) and Ketjen Black carbon (2.2 : 1 by weight) were placed in a hollow glass vial in Ar atmosphere. Then, the end of the glass vial was sealed to avoid water moisture during the infusion process. The composite contained glass vial was heated to 155 °C for 12 hours to infuse active sulfur into the pores of KB carbon and subsequently cooled to room temperature. The resulting composite had a sulfur content of 66 wt%. The sulfur infused KB composite (77 wt%) was mixed with SP (8 wt%) and 10 wt% polyvinylidene

fluoride (Sigma Aldrich) dissolved in *N*-methyl-2-prolidone (15 wt%) in *N*-methyl-2-prolidone (Sigma Aldrich), and the mixture is ball-milled at 50 rev per s for 30 minutes. The resulting viscous slurry was casted onto a carbon sprayed aluminum foil as a current collector using a doctor-blade. The coated slurry is then dried in a convection oven at 60 °C for 5 hours. The prepared electrode is cut into a circular disk, and the electrode has sulfur loading of 1.1 mg cm$^{-2}$ with 50 wt% of active sulfur per cathode. After including conductive carbon components in the clip coated separator (excluding the mass of silica nanospheres), the active sulfur content remains at 47.5%.

BMSC (Ball Milled Sulfur Cathode) – the 70 wt% sulfur powder (Sigma Aldrich) was mixed with SP (20 wt%) and 10 wt% polyvinylidene fluoride (Sigma Aldrich) dissolved in *N*-methyl-2-prolidone (15 wt%) in *N*-methyl-2-prolidone (Sigma Aldrich), and the mixture is ball-milled at 50 rev per s for 30 minutes. The resulting viscous slurry was coated onto a carbon sprayed aluminum foil as a current collector using the doctor-blade. The coated slurry is then dried in a convection oven at 60 °C for 5 hours. The prepared electrode is cut into a circular disk, and the electrode has the loading of 5 mg cm$^{-2}$ with 70 wt% of active sulfur per cathode.

VISC (Vapor Infused Sulfur Cathode) – this is a carbon–sulfur cathode created by infusion of sulfur in the vapor phase into a carbon fiber matrix.[18] Sulfur cathodes are prepared by coating the composite material onto a carbon coated Al foil. The cathode has the sulfur content of 68 wt% and loading of 5.15 mg cm$^{-2}$. After including conductive carbon components in the clip-coated separator (excluding the mass of silica nanospheres), the sulfur contents for BMSC and VISC are 69.31% and 67.35%, respectively. All measurements reported in the study utilize a cathode size of 1.26 cm$^2$.

Li metal foil was cut into a 1.27 cm diameter circular disk, and the Li metal disks are completely soaked in 0.5 M LiNO$_3$ (Sigma-Aldrich) 1,2-dimethoxyethane (DME, Sigma Aldrich) and 1,3-dioxolane (DOL, Sigma Aldrich) (1 : 1 v/v) electrolyte solutions for 24 hours for the pretreatment.[19] Then, the pretreated Li metals were rigorously dried in air/oxygen-free Ar environment. Same size of Li metal disks is used for the pristine Li anode.

Three different electrolytes are prepared for this study: (i) 1 M bis(trifluoromethane)sulfonamide lithium salt (LiTFSI, Sigma Aldrich) in DME : DOL (1 : 1 v/v) electrolyte, (ii) 1 M LiTFSI with 0.05 M LiNO$_3$ in DME : DOL (1 : 1 v/v), and (iii) 1 M LiTFSI with 0.3 M LiNO$_3$ in DME : DOL (1 : 1 v/v).

CR2032-type Li–S coin cells are assembled with the pristine/coated separators, Li metal disks, Li–S cathodes, stainless-steel springs and spacers, and the electrolytes. 40 μL of the electrolyte is used per cell. The first 20 μL of the electrolyte is added to the coating layers of the separator. Then, the cathode is placed onto the electrolyte-wetted separator facing the coating layers. Another 20 μL of the electrolyte is applied to the other side of the separator and pretreated or pristine Li metal disk is placed. Then the spacer and spring are used to sandwich the anode/separator/cathode, and pressure of 15 MPa is applied to punch the cell. The assembled cell is rested for about 15 minutes before testing. Cell assembly was carried out in an Ar filled glove-box (MBraun Labmaster). The room-temperature cycling

characteristics of the cells were evaluated under galvanostatic conditions using Neware CT – 3008 battery testers and the electrochemical process in the cells were studied by cyclic voltammetry using a CHI600D potentiostat.

## 2.4 Characterization

**Langmuir–Blodgett trough:** surface pressures of 350 nm silica colloids, MWCNT, KB, SP, and SDS surfactant are measured using conventional LB trough (KSV NIMA L & LB Troughs). The trough has dimension of 7.5 cm × 32.4 cm. The trough was cleaned using pure ethanol and DI water and fully dried with nitrogen gas. The trough was filled with DI water and a 0.5 ml of suspension is injected at the ends of the trough to float particles. After the injection of the suspension, rest time of ∼7 minutes was needed to evaporate excess ethanol from the suspension. Then the resulting floating particles are compressed at the rate of 3 mm min$^{-1}$ to collect the surface pressure profiles. For obtaining the pressure profile of LBDSC and LBS, ∼35 cm$^2$ and ∼25 cm$^2$ areas are set to mimic actual coating process that occurs at the surface from the 50 ml glass beaker.

To collect LBDSC surface profile, ∼35 cm$^2$ of the surface is saturated with the silica colloids and rested about 5 minutes to evaporate remaining ethanol. Then, 5 μL of the surfactant is added and the pressure profile is collected at the compression rate of 3 mm min$^{-1}$.

For LBS surface profiles, ∼25 cm$^2$ area is fully covered by MWCNT, KB, and SP, and without the rest time, the surface pressure profiles are collected at the compression rate of 3 mm min$^{-1}$.

The surfactant surface pressure profile is measured at four different areas (7 cm$^2$, 11 cm$^2$, 19 cm$^2$, 38 cm$^2$) without compressing the barriers, and the 5 μL of the surfactant surface pressures are measured over time.

**Galvanostatic charge/discharge.** Neware battery testing system is used to perform cycling testing of the Li–S cells. 1.5 V to 2.6 V and 1.7 V to 2.6 V voltage windows are used for without/with LiNO$_3$ electrolyte systems, respectively. 1.7 V to 2.6 V voltage window is chosen for the LiNO$_3$ system to preserve LiNO$_3$ passivation layer on the Li anode.

**CV.** CHI600D potentiostat is used to perform cyclic voltammetry analysis of the LiS cell. 0.1 mV s$^{-1}$ scan rate with the voltage window of 1.5 V to 2.6 V are used for the measurement.

**SEM.** The morphology of the coating layers on the separator is analyzed using Keck scanning electron microscope (LEO 1550 FESEM) at 3 kV acceleration voltage.

**EDXS.** Energy dispersive X-ray spectroscopy (EDXS) is performed on Keck scanning electron microscope to map the elements on the coatings on the separator.

**TGA.** Thermogravimetric analysis (TGA) was used to determine the content of sulfur in the S-KB composite. The analysis performed under nitrogen gaseous atmosphere with a heating rate of 10 °C min$^{-1}$.

**ACI.** Alternating current impedance (ACI) spectroscopy is measured using a Novocontrol N40 broadband dielectric spectroscopy.

This journal is © The Royal Society of Chemistry 2016

*J. Mater. Chem. A*, 2016, **4**, 14709–14719 | **14711**

# 3. Results and discussion

The LBSDC and LBS coating methods enable creation of well-defined layers of materials in various physical forms and chemistries on a conventional polypropylene separator, without the need for chemical binders. LBSDC is a discontinuous process (ESI Video 1†) that utilizes SDS surfactant, inducing Marangoni effect, to lower the surface tension of water and to provide a unidirectional force on floating particles or to a particulate LB film at the air/particle/water interface to form a dense, close-packed structure (ESI Video 2†). Care is needed in this step, for on the small length scales of these monolayer films the pressure provided by the surfactant can easily exceed the stability of the self-assembled LB film, causing it to rupture due to too strong surface tension gradient (Fig. S1†). Grains that exceed 200 nm in size exhibit the greatest film stability and are able to form the most densely packed coatings through the LBSDC technique. The LBS method, on the other hand, is a continuous process that uses constant injection of a particle suspension during the coating process to maintain a closely-packed LB film by a self-assembly mechanism, which is induced by the simple spreading and mixing of the water miscible fluid (ESI Video 3 and 4†). This approach enables particles smaller than 200 nm in size to be coated on a mobile substrate due to the absence of the extra surface tension gradient provided by the surfactant. The LBS method is therefore more flexible than the LBSDC method, but requires constant injection of the suspension during the coating process. Hence, LBS method is simpler and more versatile than LBSDC; however, LBSDC has more precision in terms of quantifying and sizing the LB film as the desired amount of the nanoparticle suspension can be injected/compressed whereas the LBS method requires continuous injection of the suspension to maintain the self-assembly process. Either or combination of the two methods can be used for the coating on any desired solid substrates as they both have different compatibility on coating materials and compaction mechanism. It is important to note that no film quality difference is observed for LBSDC or LBS methods.

Surface pressure profiles obtained using the LBSDC and LBS approaches to assemble monoparticle layers of ~350 nm diameter sized nanospheres and MWCNT at the air/water interface are reported in Fig. S2.† Fig. 1 compares the pressure profiles to those obtained using a conventional LB trough. Three different surface pressure points are chosen in Fig. 1a to investigate the packing densities of the colloidal film onto a separator achieved with each of the approaches. The points A, B, and C correspond to the surface pressure of 60 mN m$^{-1}$, 33 mN m$^{-1}$, and 2 mN m$^{-1}$, respectively. Points A and C represent the surface pressure where the colloids are overly packed and inadequately packed, and point B represents the starting surface pressure from the LBSDC method. The inflection point represents a transition point where the folding of the film starts, which is consistent with what is observed in the SEM images at point A. Point B shows the most uniform coating, which indicates that the surface pressure between 33 mN m$^{-1}$ and 38 mN m$^{-1}$ will yield the highest quality LB film. The
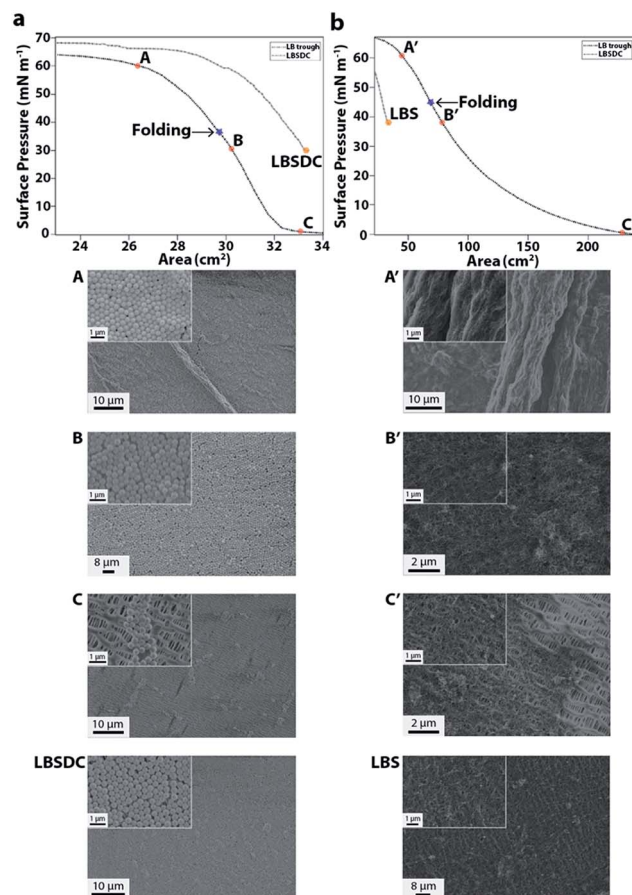


Fig. 1 Langmuir–Blodgett surface pressure profiles and corresponding coating qualities of silica nanospheres and MWCNTs at designated surface pressures. (a) Silica nanosphere surface pressure profiles of conventional LB trough and LBSDC methods with SEM images of the coating qualities at 60 mN m$^{-1}$, 33 mN m$^{-1}$, and 2 mN m$^{-1}$. (b) MWCNT surface pressure profiles of conventional LB trough and LBS methods with SEM images of the coating qualities at 61 mN m$^{-1}$, 37 mN m$^{-1}$, and 1 mN m$^{-1}$.

surface pressure profile of the colloids from the LBSDC method starts at 33 mN m$^{-1}$, which represents the amount of pressure exerted by one 5 μL drop of the 3 wt% SDS surfactant on the film. This pressure from the surface tension gradient allows the colloids to be packed closely and remain stationary, and therefore, no inflection point is observed from the LBSDC profile. To confirm the packing density of the colloids using the LBSDC method, the colloids are coated onto the separator using the LB trough at 33 mN m$^{-1}$ and using the LBSDC method. Coating quality consistent with that observed using the LBSDC approach is apparent from the SEM images, which confirms that LBSDC starts from a highly packed colloidal LB film. To understand the role of the surfactant in the LBSDC method, the maximum amount of the pressure acting on the film is measured and its stability is observed (see Fig. S3a and b†). The maximum pressure that the surfactant can provide is ~34 mN m$^{-1}$ and tends to slowly fade over time. The maximum pressure exerted by the surfactant matches the starting surface pressure of the colloids using the LBSDC method, where the

increased pressure is the same as obtained from one drop of the surfactant.

In Fig. 1b, the surface pressure profiles of the MWCNT is compared from conventional LB trough and LBS methods, and three different surface pressure points, A′, B′, and C′, are chosen at 61 mN m$^{-1}$, 37 mN m$^{-1}$, and 1 mN m$^{-1}$, respectively, to observe the coating quality. The MWCNT film tends to fold as shown in the SEM at point A′, and poor coverage of the film is seen at point C′. A long compression region of the film is observed from the profile by comparing the area before and after the inflection point. This is because of the elastic behavior of the self-assembled MWCNT film as the film is comprised of nanotubes. Based on the geometry of the particle, different trends of the surface pressure profiles can be obtained (see Fig. S3c†).

To investigate where the coating quality of the LBS lies, the surface pressure profile of the LBS method is measured and compared to the profile obtained from the LB trough. The LBS method requires a constant injection of the suspension to maintain high packing density by self-assembly mechanism induced by spreading and mixing of the suspension solvent (ethanol) with water (ESI Video 3 and 4†). To observe how much pressure is exerted during the self-assembly, the surface pressure was measured by saturating the surface of the trough with MWCNT. The measured pressure is 37 mN m$^{-1}$, which is the pressure exerted from the self-assembly. Since the spreading velocity depends on the distance traveled by the particle, the area on the trough is set to around 25 cm$^2$, which is a similar surface area for our experimental coating process. No inflection point is shown from the profile, which confirms that the fibers are closely packed and compressed from the starting point. Furthermore, congruent coating qualities are observed at point B′ and from the LBS in Fig. 1b, confirming that the LBS method yields a closely packed, high quality LB film. Moreover, surface pressure profiles of KB and SP carbons using the LB trough and LBS methods are measured to understand the stability of the film in the presence of the surfactant (see Fig. S3c†). The starting surface pressure of MWCNT, KB, and SP from the LBS method is 37 mN m$^{-1}$, 20 mN m$^{-1}$, and 35 mN m$^{-1}$, respectively. One drop of the surfactant provides an instant pressure of 34 mN m$^{-1}$, similar to that of MWCNT and SP, while exceeding that of KB. As a result, the film starts to collapse in the presence of the extra surface tension gradient. As expected, the instant destruction of the KB film, ~1 second, is observed, while a longer destruction time, ~7 seconds, is observed for MWCNT and SP in the presence of the surfactant (Fig. S1†). The above results support that the LBSDC and LBS coating methods start in an optimized packing condition and yield high-quality LB films.

Fig. 2a illustrates the simplicity and effectiveness of the LBSDC and LBS methods. The coatings and their processes are important not only because they exhibit an excellent close-packed morphology, but also because they are the thinnest and highest fidelity coating on a battery separator. For example, thickness variations for silica nanospheres and MWCNT within a single monolayer of the silica particle size and ~80 nm of MWCNT (Fig. 2b) are achieved. This means that these coatings

will add very little mass to a battery separator or electrode, yet significantly optimize the electrochemical performance in the batteries due to the uniform and densely-packed coating layers.

The polypropylene Celgard™ membrane used as a separator in the Li–S battery is chosen as a substrate to illustrate the utility of the LBSDC and LBS approach for at least three reasons. First, the rechargeable Li–S battery is arguably one of the most important platforms for storing large amounts of electrical energy at a moderate cost. The redox reaction between lithium and sulfur, $16Li + S_8 \Leftrightarrow 8Li_2S$, occurs spontaneously, is reversible, and produces up to two electrons per formula unit of sulfur, without intervention with catalysts or other means. These features endow the Li–S battery with high theoretical specific energy, 2600 W h kg$^{-1}$, and low material and operating costs.[20–22] Second, in practice Li–S cells fail to deliver on these high expectations for two stubborn, fundamental reasons: (i) sulfur and its reduction compounds with lithium are such poor conductors that unless the electrochemical reactions between Li$^+$ and sulfur occur in solution near a conductive substrate or in subnanometer-sized pores of a conductive host material such as microporous carbon, only a small fraction of the active sulfur material in the cathode is electrochemically accessible; and (ii) the reaction between Li$^+$ and S$_8$ is a multi-step reaction,[23] in which the higher molecular weight intermediate species Li$_2$S$_x$ ($x \geq 4$), collectively termed lithium polysulfides (LiPS), are soluble whereas the lower molecular weight ones ($x < 3$) are not.
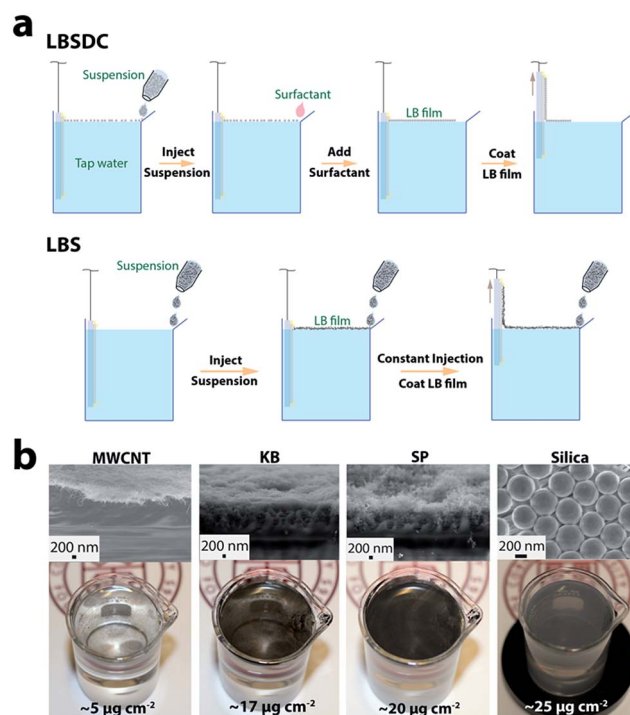


**Fig. 2** LBSDC and LBS coating methods and Langmuir–Blodgett films. (a) Schematic illustrations of LBSDC and LBS coating methods. (b) Thicknesses, self-assembled Langmuir–Blodgett films, and gravimetrical areal density of single coating layer of MWCNT, KB, SP, and silica nanospheres on the separator using LBS method. One coating layer thickness of MWCNT (~80 nm), KB (~350 nm), SP (~850 nm), and silica (~350 nm).

This journal is © The Royal Society of Chemistry 2016

*J. Mater. Chem. A*, 2016, **4**, 14709–14719 | **14713**

Dissolution of LiPS in an electrolyte means that a substantial fraction of the active material can be lost before it is fully reduced to $Li_2S$, if the LiPS diffuses too far from the conductive substrate in the cathode. An even greater concern is that once in the electrolyte, LiPS can diffuse to the lithium metal anode and undergo chemical reduction to form polysulfides of lower order, some of which are insoluble and deposit on the anode, causing time-dependent loss of both lithium and sulfur in a parasitic process termed shuttling. Finally, a variety of approaches have been investigated for controlling LiPS dissolution, diffusion, and shuttling in Li–S cells. Methods ranging from sequestering the sulfur in porous carbon structures in nanospheres,[18] nanotubes/nanofibers,[24] graphene/graphene oxide sheets[25,26] all utilize the strong affinity of sulfur for carbon-based materials to limit dissolution. Other workers have shown that strong specific interactions of LiPS with amine-containing molecular[27,28] and inorganic chalcogenide,[29] particulate additives can be used to reduce sulfur loss to the electrolyte.[30,31] Even in the best cases, however, there is a finite, equilibrium concentration of LiPS dissolved in the electrolyte such that chemical potential of LiPS in the cathode is equal to that in the electrolyte.[21,27] As a result, the dissolved LiPS are still able to diffuse to the Li anode, react with it, and increase the interfacial resistance of the anode. Hendrickson et al. showed that a substantial amount of LiPS is also lost by adsorption in the pores of the separator and that this source of loss can be removed in model Li–S cells run in a separator/membrane-free configuration, but at the price of very high interfacial impedances at the anode.[19] Other works have shown that incorporation of carbon,[32–43] metal-oxide,[44,45] and polymer[46–48] coatings on separators can reduce LiPS loss, but the electrolyte must still be reinforced with additives such as $LiNO_3$ thought to limit LiPS reaction with metallic lithium, for stable cell cycling over extended periods or in practical lithium- and electrolyte-lean Li–S cell designs.

A broad range of materials such as SP carbon,[37–39] KB carbon,[38] carbon nanofibers/tubes,[33–36] mesoporous carbon,[32] alumina[49] and graphene[40–44] were coated on Celgard, and the electrochemical performances of Li–S cells based on these separators are investigated in literatures. To note the versatility and adaptability of the developed coating methods, large selections of a material with one or more different coating materials are coated on the separator and are suitable for different substrates (Fig. S4†). The thickness of a single layer coating of MWCNT, KB, and SP is ~80 nm, ~350 nm, and ~850 nm, respectively (Fig. 2b). The corresponding gravimetric coverage of a single layer of MWCNT, KB, SP, and ~350 nm silica nanospheres is ~5 μg cm$^{-2}$, ~17 μg cm$^{-2}$, ~20 μg cm$^{-2}$, and ~25 μg cm$^{-2}$, respectively (Fig. 2b).

The negligible weight gained per coating layer with high uniformity is best appreciated by comparison to literature results, where carbon materials are coated using the vacuum filtration[33–35] (loading: 0.17 to 0.35 mg cm$^{-2}$, thickness: 20 to 25 μm) or doctor-blade[32,37,38] (loading: 0.26 to 0.53 mg cm$^{-2}$, thickness: 6.7 to 27 μm) methods. As illustrated in Fig. S4b,† LBS coatings on Celgard are single-sided and exhibit high mechanical strength absence of chemical binders. The effectiveness of LBS-coated Celgard comprised of 1–10 coating layers

of silica nanospheres, MWCNT, KB, and SP were systematically studied for their ability to improve cycling behavior in Li–S cells. As shown in Fig. S5,† Li–S cells based on the carbon coated separator yield superior capacity and retention rates, compared with pristine Celgard separator. Specifically, the capacity retention after 100 cycles is improved from 31% for the pristine separator to 63%, 71%, 63%, and 49% for ten coating layers of MWCNT, KB, SP, and silica nanospheres, respectively. The initial capacity for the pristine separator, 10LR MWCNT, 10LR KB, 10LR SP, and 10LR are 1067 mA h g$^{-1}$, 1535 mA h g$^{-1}$, 1594 mA h g$^{-1}$, 1541 mA h g$^{-1}$, and 1588 mA h g$^{-1}$, respectively at 0.5C for the first four and 0.2C for the last.

Our results show that carbon-coated Celgard is more effective than the silica-coated material in stabilizing capacity retention of Li–S cells. We attribute this behavior to the stronger adsorption of LiPS on the $SiO_2$ coating layer by physical and covalent bonds[30] and the inability to utilize the trapped LiPS. As we observe in Fig. S5a,† ten layers silica-coated separator LiS cells show increase in coulombic efficiency approximately 90% after 100$^{th}$ cycles whereas the all carbon coated separators exhibit lower efficiency values. This verifies that silica coatings are effective in terms of suppressing LiPS shuttling; however, severe capacity fading at initial cycles is observed due to silica's inability to reutilize the adsorbed LiPS at the surface. Moreover, our results also confirm observations reported by Yao et al.,[38] that MWCNT and KB are particularly effective as separator coatings because the interconnected porous structure of coatings based on these carbon materials allow for both trapping of LiPS and utilization of the trapped materials in electrochemical cycling. It is important to note, however, that the weight of MWCNT per coating layer is only 25% that of KB, implying that the MWCNT coating is by far the most efficient of the carbon materials studied.

A separator coating design that offers a combination of the strong LiPS binding attributes of a close-packed array of $SiO_2$ particles and high utilization of trapped LiPS evident for MWCNT would seem ideal for Li–S cells. This perspective is at odds with the work of Yao et al.,[38] which previously demonstrated that a LiS battery separator coated with a mixture of ceramic nanoparticles and SP carbon, using the doctor-blade coating method, yields cells with poorer electrochemical performance than those in which a simple SP coating layer was used.

Here, we take advantage of the spatial control afforded by the LBS and LBSDC coating strategy to create a multifunctional separator coating with the configuration shown in Fig. 3a. In this so-called *clip* configuration multiple layers of closely packed silica particles are surrounded by a conductive fibrous network based on MWCNT. The location of the silica layer is designed such that under compression in a battery, the two MWCNT coatings contact each other (like the clasps of a clip) and also make contact with the cathode so as to ensure maximum electrochemical access to LiPS trapped in any of the coating layers that comprise the clip. As a proof of concept, we created and studied clip coating designs comprised of five coating layers of MWCNT and three monolayers of silica. The quality and mechanical strength of these coatings are

**14714** | *J. Mater. Chem. A*, 2016, **4**, 14709–14719

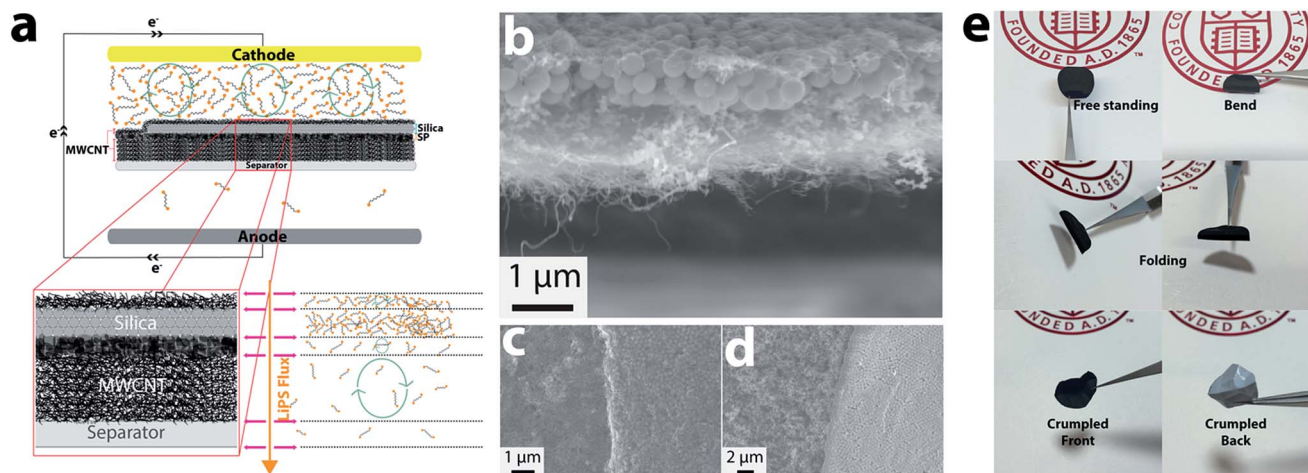This journal is © The Royal Society of Chemistry 2016

Fig. 3 Clip configuration coatings on the separator. (a) Clip configuration architecture design and LiPS flux diagram across the separator during the discharge of Li–S cell. (b) Cross-sectional SEM image of the clip coated separator. (c) SEM image of the clip coated separator at the silica–SP boundary layer. (d) SEM image of the clip coated separator at the boundary without final MWCNT coating. (e) Mechanical strength of the clip coated separator.

illustrated in Fig. 3b–e. Fig. 3b shows the cross section of the clip configuration, where it is seen that the material has a consistent structure and a thickness of ~3 μm. The clip configuration of the coating has also been confirmed by SEM image at the silica–carbon layer boundary (Fig. 3d). Fig. 3c then shows a uniform thin fibrous morphology of the coating surface after the final layer of MWCNT coverage is established over the three layers of silica nanosphere film. We observed the immersion of close-packed silica layers at the third layer on top of the SP layer of the clip coating (Fig. 3d). For reference, one monolayer of silica nanospheres is also shown in Fig. S6.†

In order to investigate the electrochemical performance of the clip-coated separator, three different cathodes, infused sulfur cathode (ISC), vapor infused sulfur cathode (VISC), and ball-milled sulfur cathode (BMSC), have been used in this study. Fig. 4a reports results from galvanostatic cycling studies of the clip separator in a 1 M LiTFSI DOL/DME electrolyte and with ISC. As we observe in Fig. 4a, in the control case with the pristine (uncoated) separator, the capacity dropped to 360 mA h g$^{-1}$ after 100 cycles at a current rate of 0.5C (838 mA g$^{-1}$). However, when the separator was coated using the aforementioned clip configuration, the clip coated separator Li–S cells without any additives exhibits initial discharge capacity of 1470 mA h g$^{-1}$ with the reversible capacity of 1210 mA h g$^{-1}$ and the capacity retention rate of 82% at 100$^{th}$ cycle with 0.5C rate. The cells with the clip coated separators also exhibit superior performance at high current rates. Initial capacities of ~1400 mA h g$^{-1}$ were obtained at 1C and 2C. Fig. 4b reports the corresponding voltage profiles at different cycle numbers for the clip configuration at 0.5C. Two discharge plateaus can be seen over many cycles: the first plateau at 2.37 V corresponds to the reduction of the elemental sulfur to high order LiPS, whereas the second plateau at 2.08 V indicates the high order LiPS reduction into low order LiPS. The voltage profiles for the clip coated (various C rates) and uncoated separator (various cycles) control are provided in Fig. S7.† It is clear that the voltage plateaus for the

discharge and charge processes does not change when the current is increased by 2 or 4 times for the clip coated separators.

To enhance the coulombic efficiency (CE) of the LiS cells, we have used pretreated lithium metal anode (see Fig. S8†) as reported in reference,[19] by soaking it in an electrolyte containing LiNO$_3$ for 24 hours followed by rigorous drying in an Ar environment. By using the pretreated Li metal anode, ~99.9% CE are achieved (see Fig. S8†). The corresponding voltage profiles are shown in Fig. S9.† To facilitate comparisons with literature results, we also performed studies using a conventional Li–S electrolyte containing 0.05 M LiNO$_3$ as the additive, and the results are shown in Fig. S10† and corresponding voltage profiles are shown in Fig. S11.†

Fig. 4c reports the rate capability of the cells with the clip coated separator are also significantly improved (for both low, ISC, and high, VISC, sulfur loading cathodes), illustrating that the capacity of the cells can recover after high rate cycles of 1C, 2C, and 3C for 10 cycles respectively. Cyclic voltammograms shown in Fig. 3d further confirms the stability of the cells in the additive-free electrolyte with pristine Li anode. The discharge and charge peaks are observed to remain at the same position over many cycles, indicative of the stable and reversible electrochemical reaction of sulfur. Furthermore, Fig. S12† show electrochemical performance of the clip coated/pristine separators with VISC in 0.3 M LiNO$_3$ and no LiNO$_3$ additive in the electrolyte. VISC has areal sulfur loading of 5.15 mg cm$^{-2}$ and a content of 68 wt%. Fig. S12a and b† show effectiveness of the clip coated separator with VISC, and increasing capacity at first several cycles can be observed as reported in literature[50] for high loadings of sulfur with a upper current collector. The clip coated separators with VISC shows reversible capacity of 1050 mA h g$^{-1}$ and capacity retention rate of 83% for 100 cycles without any additives in the system. Also, Fig. S13† shows the series of the voltage profiles of Li–S cells with the clip coated/pristine separators and VISC in the electrolyte with/without LiNO$_3$. More, the
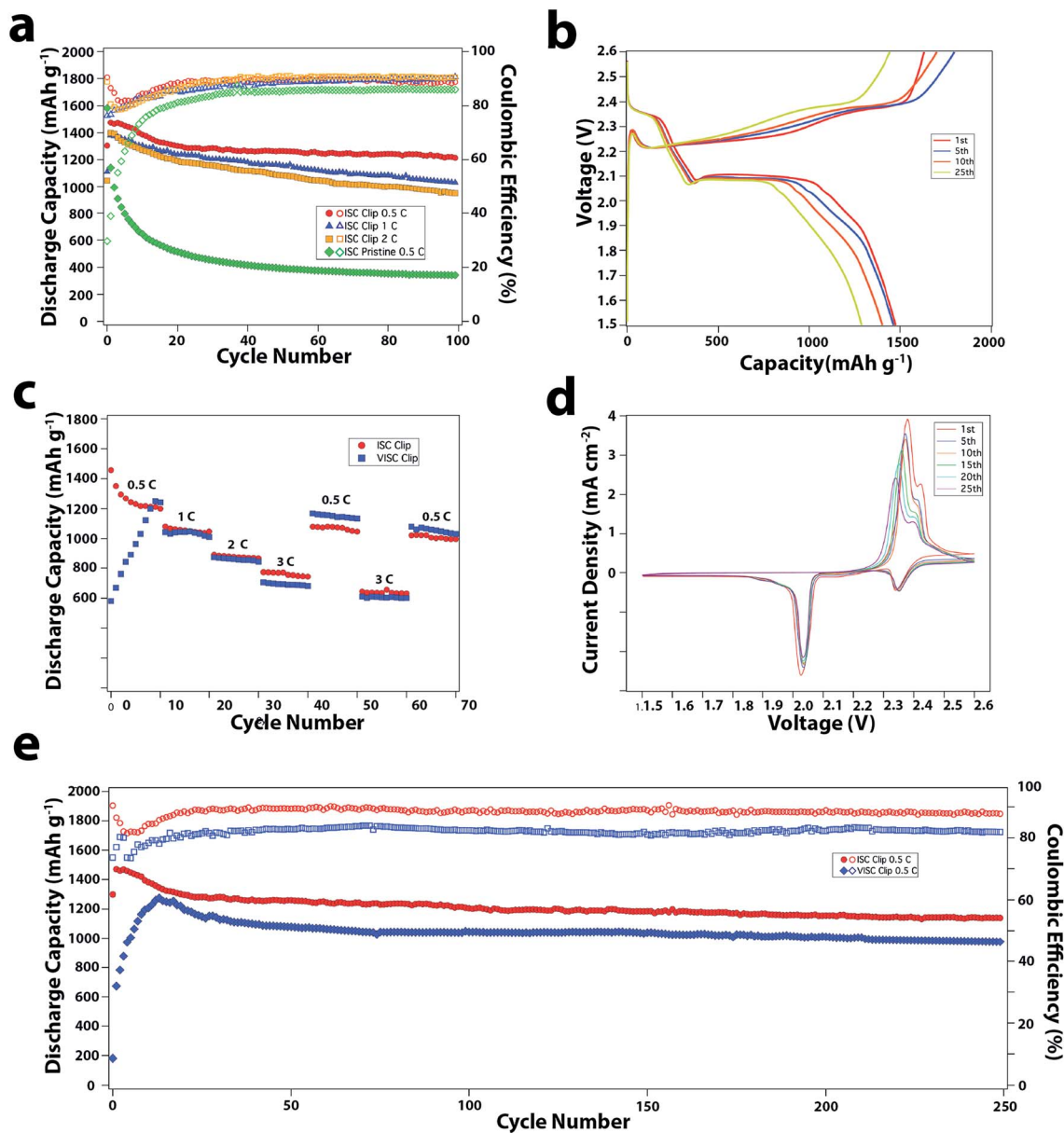
Fig. 4  Electrochemical performance of the clip coated separators without LiNO₃. (a) Cycling performance of pristine Li anode Li–S cell with/without the clip coated separator and with ISC at three different C rates. (b) Discharge–charge voltage profiles of the corresponding Li–S cell with the clip coated separator and ISC for various cycles at 0.5C. (c) Cycling performance of pristine Li anode with the clip coated separator Li–S cells with ISC and VISC at various C rates. (d) Cyclic voltammograms of the pristine Li anode with the clip coated separator Li–S cell with ISC at 0.1 mV s⁻¹ for various cycles. (e) Cycling performance of the clip coated separator Li–S cells with ISC and VISC at 0.5C for 250 cycles.

clip coated separators are also tested in a harsh environment – BMSC which is made *via* simple ball-milling sulfur powder with a carbon matrix and has a high sulfur loading of 5 mg cm⁻² and 70% (Fig. S14†). The clear improvements of the electrochemical performance of Li–S with the clip coated separators, the reversible capacity of ~700 mA h g⁻¹ with 90% capacity retention for 100 cycles, are shown considering the mass loading of the clip coated separator, ~130 μg cm⁻², and the conditions of the cathode. Fig. S15† shows the series of the voltage profiles of Li–S cells with the clip coated/pristine separators and BMSC in the electrolyte with/without LiNO₃. Overall, the electrochemical performance of the clip coated separators are thoroughly

examined using pretreated/pristine Li anode, various cathodes, and the electrolyte with/without LiNO₃, and good electrochemical performance of the Li–S cells with the clip coated separators are achieved. Overall, the electrochemical performance of the clip coated separators are thoroughly examined using pretreated/pristine Li anode, various cathodes, and the electrolyte with/without LiNO₃, and good electrochemical performance of the Li–S cells with the clip coated separators are achieved. Longer cycling performance of clip coated separators with ISC and VISC without LiNO₃ in the electrolyte is shown in Fig. 4e, and stable performance, >1000 mA h g⁻¹ and ~80% capacity retention rate, is observed over 250 cycles at 0.5C,
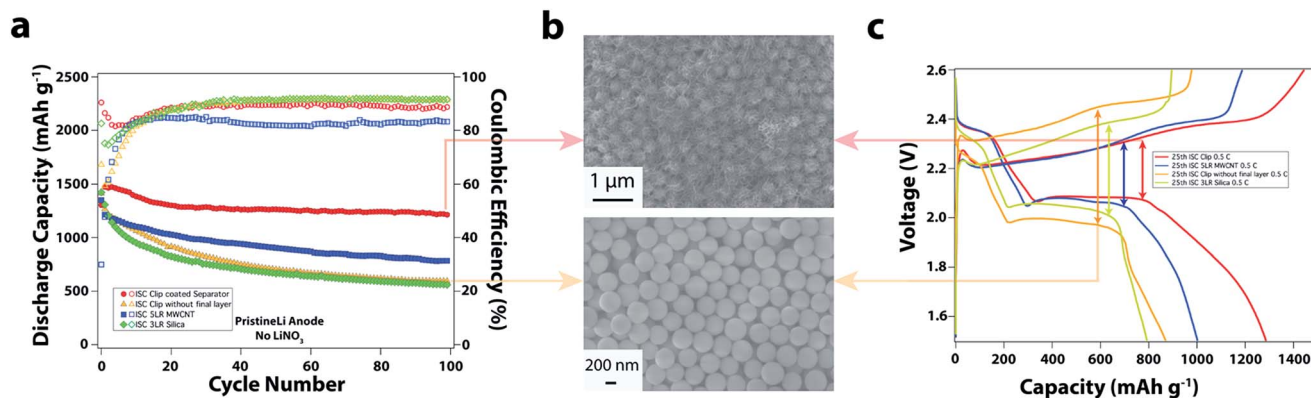
14716 | *J. Mater. Chem. A*, 2016, **4**, 14709–14719

This journal is © The Royal Society of Chemistry 2016

**Fig. 5** Electrochemical analysis of the clip layer parts. (a) Cycling performance of the pristine Li anode with the clip coated separator, clip coated separator without final MWCNT layer (same structure as shown in Fig. 4d), five layers of MWCNT coated separator, and three monolayers of silica nanospheres coated separator Li–S cell with ISC at 0.5C. (b) SEM images of the clip coated separator (top) and without final layer of MWCNT (bottom). (c) Discharge–charge voltage profiles of pristine Li anode with clip coated separator, clip coated separator without final MWCNT layer, five layers of MWCNT coated separator, and three monolayers of silica nanospheres coated separator Li–S cell with ISC for 25th cycle at 0.5C.

which is remarkable with such high sulfur loading and $LiNO_3$ free electrolyte.

In order to investigate the effect of each compartment in the clip configuration, we compared the electrochemical performance of the clip with five layers of MWCNT coating, three layers of silica, and a clip configuration without the final electrical path MWCNT layer (see Fig. 5a), which is the equivalent structure shown in Fig. 5b. Significantly, it is noted that without the final MWCNT coating to complete the clip, similar electrochemical performances are observed in Li–S cells using the multifunctional MWCNT-$SiO_2$ coatings, compared to those based on separators coated with three monolayers of silica. These results underscore the importance of the clip configuration in complementing LiPS adsorption achieved with $SiO_2$ coatings, with utilization of the trapped LiPS made possible by the MWCNT coating layers. They also validate our hypothesis that a good electrical conductive path is required to efficiently entrap and utilize dissolved LiPS. Fig. 5c compares the voltage profiles of the cell with the clip configuration done in different steps. Consistent with the previous observation, the capacity is seen to increase progressively as the clip components are sequentially added to complete the structure: 561 mA h g$^{-1}$ at 100$^{th}$ cycle, 596 mA h g$^{-1}$ at 100$^{th}$ cycle, 785 mA h g$^{-1}$ at 100$^{th}$ cycle, and 1214 mA h g$^{-1}$ at 100$^{th}$ cycle when 3LR silica, the multifunctional MWCNT-$SiO_2$, 5LR MWCNT, and clip are coated on the separator, respectively. Another important observation is that the overpotential of the cell substantially declines when the final layer is involved, which confirms our hypothesis that the silica surface traps LiPS in the separator, which overtime reduces the electrolyte conductivity. Reutilization of the LiPS in the clip configuration eliminates this problem and reduces the overpotential correspondingly.

Finally, we investigated the morphology of the coating surface on the clip-coated separator after cycling using SEM. Fig. 6a shows the morphology of the cross sectional separator after 10$^{th}$ discharge and corresponding energy-dispersed X-ray spectroscopy (EDXS) measurements of elemental mapping of

carbon, sulfur, and silicon, in which silicon layer and sulfur distribution in the clip structure is clearly seen. The low X-ray intensity for carbon is due to high coverage of sulfur after the discharge, indicating carbon layers are efficiently trapping dissolved LiPS. The structure of the clip coating is preserved upon discharge and charge, indicating the robust properties of the coating in both mechanical and chemical aspects. Also EDXS measurements of top view of the clip coated separator show a uniform distribution of carbon and sulfur elements (Fig. 6b).
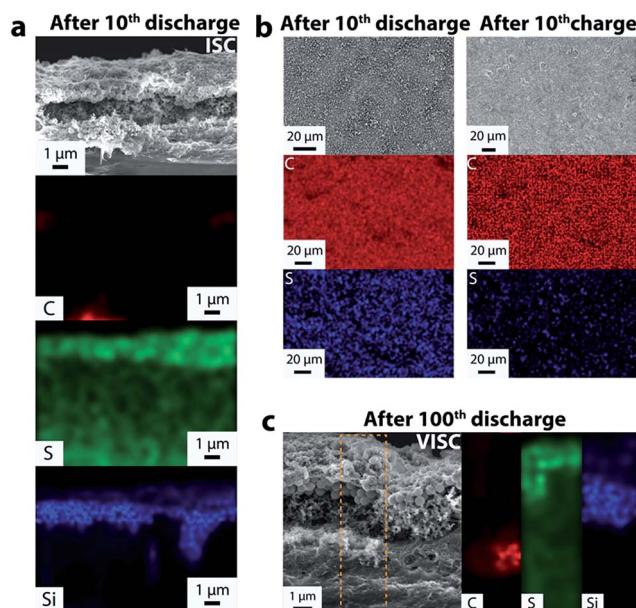


**Fig. 6** Clip coated separator morphology and elemental mappings after several cycles. (a) Cross sectional SEM image of the clip coated separator with ISC after 10$^{th}$ discharge with carbon, sulfur, and silicon maps. (b) Top view SEM image of the clip coated separator with ISC after 10$^{th}$ discharge/charge with carbon and sulfur maps. (c) Cross sectional SEM image of the clip coated separator with VISC after 100$^{th}$ discharge with carbon, sulfur, and silicon maps.

This journal is © The Royal Society of Chemistry 2016

*J. Mater. Chem. A*, 2016, **4**, 14709–14719 | **14717**

The fact that the amount of sulfur decreased during the charge process further substantiates the ability of the coating to reutilize the adsorbed species. In addition, the morphology of the clip coated separator with VISC after 100th cycles is shown in Fig. 6c. This double confirms that the multifunctional coatings remain robust after large number of cycles with the presence of high loading and content of sulfur in the Li–S cells. We have also observed decrease in internal resistance of the Li–S cell for clip coated separator compared to pristine separator (see Fig. S16†). The decreased impedance indicated that the clip design is able to facilitate the electron transfer even the insulating silica particles are involved. The summary of electrochemical performance of LiS cell configurations are mentioned in ESI Table S1.†

## 4. Conclusions

In summary, we have demonstrated two new versatile coating methods, LBSDC and LBS, for creating surface films that utilize the surface tension gradient to create well-ordered monolayer films at an air/water interface. The methods allow multifunctional coatings to be created in a range of designs using a wide selection of individual materials, as well as material combinations, on a variety of substrates, without the need for chemical binders. The utility of the approach is illustrated using the polypropylene membrane separator, Celgard, commonly employed in Li–S batteries as a substrate. Through systematic studies, it is shown how mono-functional coatings based on different metal oxides and carbon influence reutilization of dissolved lithium polysulfide species. An unusual coating configuration termed the "clip", created by stacking an incomplete, but well-formed layer of $SiO_2$ particles between two complete layers of carbon is used to illustrate both the versatility of the method to create multifunctional coatings with good spatial control and the effectiveness of such coatings in battery separators. In particular, the clip coated separator is observed to exhibit largely improved active material utilization, enhanced capacity retention over extended charge/discharge cycling, and attractive high rate capability. These observations are explained in terms of the ability of the multifunctional coatings to simultaneously adsorb and trap LiPS created at the cathode, without losing electrochemical access to the materials. The new coating approach and configurational design of coating materials synergistically work together to advance Li–S cells and allow us to investigate and optimize the different coating structures.

## Acknowledgements

## Notes and references

1 H. Kuhn, D. Mobius and H. Bucher, *Early days of molecular electronics*, 3b, 1972, vol. 1, pp. 577–702.
2 E. Delamarche, B. E. Delamarche, B. Michel, B. Michel, H. a. Biebuyck and H. a. Biebuyck, *Adv. Mater.*, 1996, **8**, 719–729.
3 E. Meyer, L. Howald, R. M. Overney, H. Heinzelmann, J. Frommer, H.-J. Guntherodt, T. Wagner, H. Schier and S. Roth, *Nature*, 1991, **349**, 398–400.
4 M. Gleiche, L. Chi and H. Fuchs, *Nature*, 2000, **403**, 173–175.
5 X. Chen, S. Lenhert, M. Hirtz, N. a. N. Lu and H. Fuchs, *Acc. Chem. Res.*, 2007, **40**, 393–401.
6 X. Li, G. Zhang, X. Bai, X. Sun, X. Wang, E. Wang and H. Dai, *Nat. Nanotechnol.*, 2008, **3**, 538–542.
7 L. J. Cote, F. Kim and J. Huang, *J. Am. Chem. Soc.*, 2009, **131**, 1043–1049.
8 J. Huang, F. Kim, A. R. Tao, S. Connor and P. Yang, *Nat. Mater.*, 2005, **4**, 896–900.
9 S. Paul, C. Pearson, A. Molloy, M. a. Cousins, M. Green, S. Kolliopoulou, P. Dimitrakis, P. Normand, D. Tsoukalas and M. C. Petty, *Nano Lett.*, 2003, **3**, 533–536.
10 P. Yang, *Nature*, 2003, 243.
11 F. Kim, S. Kwan and J. Akana, *J. Am. Chem. Soc.*, 2001, **123**, 4360–4361.
12 S. Murata, N. Kuriyama and M. Kushida, *Thin Solid Films*, 2015, **589**, 115–119.
13 H. L. Nie, X. Dou, Z. Tang, H. D. Jang and J. Huang, *J. Am. Chem. Soc.*, 2015, **137**, 10683–10688.
14 J. Huang, A. R. Tao, S. Connor, R. He and P. Yang, *Nano Lett.*, 2006, **6**, 524–529.
15 Y. Lu, Y. Yang, A. Sellinger, M. Lu, J. Huang, H. Fan, R. Haddad, G. Lopez, A. R. Burns, D. Y. Sasaki, J. Shelnutt and C. J. Brinker, *Nature*, 2001, **410**, 913–917.
16 Q. Cao, S. Han, G. S. Tulevski, Y. Zhu, D. D. Lu and W. Haensch, *Nat. Nanotechnol.*, 2013, **8**, 180–186.
17 L. M. Rossi, L. Shi, F. H. Quina and Z. Rosenzweig, *Langmuir*, 2005, **21**, 4277–4280.
18 N. Jayaprakash, J. Shen, S. S. Moganty, A. Corona and L. A. Archer, *Angew. Chem.*, 2011, **50**, 5904–5908.
19 K. E. Hendrickson, L. Ma, G. Cohn, Y. Lu and L. A. Archer, *Adv. Sci.*, 2015, **2**, 68–77.
20 X. Ji, K. T. Lee and L. F. Nazar, *Nat. Mater.*, 2009, **8**, 500–506.
21 L. Ma, K. E. Hendrickson, S. Wei and L. A. Archer, *Nano Today*, 2015, **10**, 315–338.
22 A. Manthiram, Y. Fu, S. Chung, C. Zu and Y. Su, *Chem. Rev.*, 2014, **114**, 11751–11787.
23 C. Barchasz, F. Molton, C. Duboc, J. C. Leprêtre, S. Patoux and F. Alloin, *Anal. Chem.*, 2012, **84**, 3973–3980.
24 X. B. Cheng, J. Q. Huang, Q. Zhang, H. J. Peng, M. Q. Zhao and F. Wei, *Nano Energy*, 2014, **4**, 65–72.
25 H. Wang, Y. Yang, Y. Liang, J. T. Robinson, Y. Li, A. Jackson, Y. Cui and H. Dai, *Nano Lett.*, 2011, **11**, 2644–2647.
26 W. Zhou, H. Chen, Y. Yu, D. Wang, Z. Cui, F. J. Disalvo, C. Biology, N. York and U. States, *ACS Nano*, 2013, **7**, 8801–8808.

**14718** | *J. Mater. Chem. A*, 2016, **4**, 14709–14719

This journal is © The Royal Society of Chemistry 2016

27  L. Ma, H. Zhuang, Y. Lu, S. S. Moganty, R. G. Hennig and L. A. Archer, *Adv. Energy Mater.*, 2014, **4**, 390–399.

28  L. Ma, H. L. Zhuang, S. Wei, K. E. Hendrickson, M. S. Kim, G. Cohn, R. G. Hennig and L. A. Archer, *ACS Nano*, 2015, **10**, 1050–1059.

29  L. Ma, S. Wei, H. L. Zhuang, K. E. Hendrickson, R. G. Hennig and L. A. Archer, *J. Mater. Chem. A*, 2015, **3**, 19857–19866.

30  S. Evers, T. Yim and L. F. Nazar, *J. Phys. Chem. C*, 2012, **116**, 19653–19658.

31  X. Ji, S. Evers, R. Black and L. F. Nazar, *Nat. Commun.*, 2011, **2**, 325.

32  J. Balach, T. Jaumann, M. Klose, S. Oswald, J. Eckert and L. Giebeler, *Adv. Funct. Mater.*, 2015, **25**, 5285–5291.

33  S. H. Chung, P. Han, R. Singhal, V. Kalra and A. Manthiram, *Adv. Energy Mater.*, 2015, **5**, 1500738.

34  S. H. Chung and A. Manthiram, *Adv. Funct. Mater.*, 2014, **24**, 5299–5306.

35  S. H. Chung and A. Manthiram, *Phys. Chem. Lett.*, 2014, **5**(11), 1978–1983.

36  G. Wang, Y. Lai, Z. Zhang, J. Li and Z. Zhang, *J. Mater. Chem. A*, 2015, **3**, 7139–7144.

37  Z. Zhang, Y. Lai, Z. Zhang and J. Li, *Solid State Ionics*, 2015, **278**, 166–171.

38  H. Bin Yao, K. Yan, W. Li, G. Zheng, D. Kong, Z. W. Seh, V. K. Narasimhan, Z. Liang and Y. Cui, *Energy Environ. Sci.*, 2014, **7**, 3381.

39  H. Wei, B. Li, Y. Zuo and D. Xia, *ACS Appl. Mater. Interfaces*, 2014, **6**, 20276–20281.

40  F. Li, G. Zhou, S. Pei, L. Li, D. W. Wang, S. Wang, K. Huang, L. C. Yin and H. M. Cheng, *Adv. Mater.*, 2014, **26**, 625–631.

41  Y. Zhang, L. Miao, J. Ning, Z. Xiao, L. Hao, B. Wang and L. Zhi, *2D Mater.*, 2015, **2**, 024013.

42  R. Fang, G. Zhou, S. Pei, F. Li and H.-M. Cheng, *Chem. Commun.*, 2015, **51**, 3667–3670.

43  W. Lin, Y. Chen, P. Li, J. He, Y. Zhao, Z. Wang, J. Liu, F. Qi, B. Zheng, J. Zhou, C. Xu and F. Fu, *J. Electrochem. Soc.*, 2015, **162**, 1624–1629.

44  Z. Xiao, Z. Yang, L. Wang, H. Nie, M. Zhong, Q. Lai, X. Xu, L. Zhang and S. Huang, *Adv. Mater.*, 2015, **27**, 2891–2898.

45  Q. Xu, G. C. Hu, H. L. Bi and H. F. Xiang, *Ionics*, 2014, **21**, 981–986.

46  Y. Chen, N. Liu, H. Shao, W. Wang, M. Gao, C. Li, H. Zhang, A. Wang and Y. Huang, *J. Mater. Chem. A*, 2015, **3**, 15235–15240.

47  Z. Zhang, Z. Zhang, J. Li and Y. Lai, *J. Solid State Electrochem.*, 2015, **19**, 1709–1715.

48  J.-Q. Huang, Q. Zhang, H.-J. Peng, X.-Y. Liu, W.-Z. Qian and F. Wei, *Energy Environ. Sci.*, 2014, **7**, 347.

49  Z. Zhang, Y. Lai, Z. Zhang, K. Zhang and J. Li, *Electrochim. Acta*, 2014, **129**, 55–61.

50  C. H. Chang, S. H. Chung and A. Manthiram, *Small*, 2016, **12**, 174–179.